Journal of Intelligent Material Systems and Structures

Original Article

Journal of Intelligent Material Systems and Structures
2018, Vol. 29(5) 969–985

DOI: 10.1177/1045389X17730659
journals.sagepub.com/home/jim
SAGE

Ultrasonic guided wave propagation in composites including damage using high-fidelity local interaction simulation

Guoyi Li, Rajesh Kumar Neerukatti and Aditi Chattopadhyay

Abstract

Composite materials are used in many advanced engineering applications because of high specific strength and stiffness. Their complex damage mechanisms and failure modes, however, are still not well-understood, thus challenging the application safety. Ultrasonic guided waves are promising structural health monitoring tools used to determine the operational safety of composite materials. In this article, a fully coupled numerical simulation model is used to study wave propagation and dispersion in composites under varying sensor locations, propagating orientations, excitation frequencies, and damage locations. The model is based on the local interaction simulation approaches/sharp interface model wherein output sensor signals are processed using the matching pursuit decomposition algorithm to study the signal features in the time–frequency domain. The changes in signals due to varying damage locations with respect to the through-thickness direction are studied under anti-symmetrical and symmetrical excitation scenarios. The results show that the signal from symmetric excitation is more sensitive to the damage location, while the signal from anti-symmetric excitation is less dispersive. It indicates that comprising effective feature extraction technique with the accurate physics-based numerical simulation model can be implemented to develop robust structural health monitoring framework for composites.

Keywords

Composite material, guided wave propagation, numerical modeling, wave attenuation, wave dispersion, damage, structural health monitoring

Introduction

Due to their low weight and high strength, composite materials and structures are widely accepted today as a material choice in a wide range of mechanical, aerospace, and civil engineering applications (Thostenson et al., 2002). Composite materials, however, are prone to multiple structural damages, for example, matrix cracks and delaminations (Corigliano, 1993; Todoroki et al., 2006), a drawback that challenges their range of reliable applicability. As such, a robust structural health monitoring (SHM) framework that can monitor the structural health of composites to enhance their safety and lifetime efficacy is needed. Among SHM techniques, the ultrasonic guided wave based method is a well-proven tool that has been used to analyze the integrity of plate-like structures (Farrar and Worden, 2007; Giurgiutiu, 2007; Lu et al., 2006; Mohanty et al., 2010; Raghavan and Cesnik, 2007; Staszewski et al., 2007). More recently, methods based on nonlinear ultrasonic guided waves were used for damage detection in metallic structures (Chillara and Lissenden, 2014; Pruell et al., 2009; Seaton et al., 1985). The use of aforementioned techniques for composites, however, is limited due to the challenges associated with the dispersive nature of the media itself. Unlike isotropic and homogeneous materials, wave propagation in an anisotropic material is associated with a multitude of complexities, such as attenuation, dispersion, and mode conversion, making the interpretation of wave behaviors based on sensor signals from the complex geometries and different layups in the composite materials and structures a

School for Engineering of Matter, Transport & Energy, Arizona State University, Tempe, AZ, USA

Corresponding author:
Aditi Chattopadhyay, School for Engineering of Matter, Transport & Energy, Arizona State University, Tempe, AZ 85287, USA.
Email: aditi@asu.edu

challenging task (Liu et al., 2010; Neerukatti et al., 2014, 2016).

Since experimental characterization and testing of every wave propagation scenario under all potential loading and environmental conditions is not practical, a physics based modeling approach is needed to more effectively and efficiently understand the mechanism of guided wave propagation in anisotropic composite materials. However, for the simulation technique to be effective, it must accurately model the system architecture, including material discontinuities, different types of damage scenarios, and actuators and sensors, that influences the dynamic response of the host structure. The methodology must account for the two-way field coupling between the transducers and the host structure and simulate the guided wave across sharp boundaries and interfaces.

The finite element method (FEM) is a well-accepted modeling technique and has been traditionally used to study wave propagation behavior in anisotropic structures (Koshiba et al., 1984; Talbot and Przemieniecki, 1975; Zienkiewicz et al., 2013). When using the FEM method, the mesh must be fine enough to generate a high-frequency wave with a small wavelength in response to a structural damage resulting in increased computational time. Other finite element (FE) based modeling techniques, such as multi-physics finite element method (MP-FEM) (Gresil and Giurgiutiu, 2013), extended finite element method (XFEM) (Liu et al., 2013), and wavelet spectral finite element (WSFE) (Ali et al., 2005), can be used to simulate wave propagation while considering the damping effects, transducer–structure coupling, and small structural defects. The computational intensity, however, increases dramatically with mesh fineness and the use of additional subroutines. Another technique that has gained recent acceptance in the non-destructive evaluation (NDE)/SHM community, especially for the simulation of guided waves in composite structures in the presence of damage, is the elastodynamic finite integration technique (EFIT) (Leckey et al., 2014; Marklein, 1999; Rudd et al., 2007). However, this technique does not used to simulate wave propagation in the complex structures. Meanwhile, analytical approaches such as the global matrix (GM) method (Obenchain and Cesnik, 2013) and transform matrix (TM) method (Nayfeh, 1991) have also been used to investigate the output signals and dispersion curves of plate-like composites. However, the analytical approach falls short because it not only fails to explicitly model the local damages and structural complexities but also does not take into consideration the electromechanical coupling between sensors and host structures.

Borkowski et al. (2013) developed an efficient, three-dimensional electromechanical elastodynamical model with two-way coupled electromechanical and electromagnetic field equations using the local interaction simulation approach (LISA)/sharp interface model (SIM) (Delsanto et al., 1992, 1994, 1997; Nadella and Cesnik, 2013). The computational efficiency of this model has proven to be significantly higher than traditional FEM approaches. The method also allows the simulation of wave propagation across sharp material boundaries without incurring significant numerical error caused by the smearing or averaging of material properties across cell interfaces. The methodology can be used to characterize the behavior of guided waves in composites under a wide range of model parameters (material properties, excitation frequencies, damage locations, etc.).

In this article, the LISA/SIM model is extended to simulate guided wave propagation in composite materials with damages in different layers. A virtual SHM platform that includes signal generation, signal conversion, time–frequency (TF) based signal processing, supervised learning based feature extraction, and damage identification is developed. Collocated lead zirconate titanate (PZT) actuators are used to generate the zero-order symmetric (S0) and anti-symmetric (A0) propagation modes, selectively. The output signal is captured using multiple sensors placed at different distances and orientations with respect to the actuators. The matching pursuit decomposition (MPD) methodology (Mallat and Zhang, 1993), which is an advanced TF based signal processing technique, is used to accurately and more efficiently decompose the sensor signal. Time of flight (ToF) and amplitude of sensor signals are extracted to study signal attenuation with distance and propagation angle in unidirectional (UD), cross-ply (XP), and quasi-isotropic (QI) laminates. Dispersion curves are evaluated for carbon fiber reinforced polymer (CFRP) and glass fiber reinforced polymer (GFRP) composites. The simulation results are validated by comparing them with published experimental work (Ono and Gallego, 2012; Pohl et al., 2010). Then, with the same plate geometry and sensor placement, the damage is modeled explicitly and the changes in signal between healthy plate and damaged plate are compared. The effect of the damage location in different layers on the output sensor signal is further investigated, and the ToF and mode amplitude are compared at different through-thickness locations under symmetric and anti-symmetric excitation modes to evaluate the guided wave sensitivity to damage.

Modeling approach

Although the LISA/SIM formulation has been derived for wave propagation simulation (Delsanto, 1998; Kijanka et al., 2013; Nadella and Cesnik, 2013; Paćko et al., 2012), very few studies have been conducted by accounting for the coupled electromechanical relation between host structure and PZTs. Accounting explicitly

for the physics of piezoelectric actuation and sensing using the LISA/SIM numerical methodology requires the derivation of a set of incremental equations for the solution of a three-dimensional coupled electromechanical elastodynamic wave propagation model. The coupled formulation was originally derived by Borkowski et al. (2013) and will be briefly presented in this section. The governing equations for a linear piezoelectric material can be written as

$$\sigma_{ij} = C_{ijkl}\varepsilon_{kl} - e_{kij}E_k \tag{1}$$

where σ_{ij}, C_{ijkl}, ε_{kl}, e_{kij}, and E_k are the second-order stress tensor, fourth-order stiffness tensor, second-order strain tensor, third-order piezoelectric tensor, and first-order electric field tensor, respectively. The electric displacement vector, D_i, is written as

$$D_i = e_{ijk}\varepsilon_{jk} - \kappa_{ij}E_j \tag{2}$$

where D_i is the first-order electric displacement tensor and κ_{ij} is the second-order dielectric tensor. The strain tensor is written as

$$\varepsilon_{jk} = \frac{1}{2}(u_{k,l} + u_{l,k}) \tag{3}$$

The electric field can be obtained from the electric potential ϕ_k as

$$E_k = -\phi_k \tag{4}$$

By combining the equations above, the stress tensor can be rewritten as

$$\sigma_{ij} = C_{ijkl}u_{k,l} + e_{kij}\phi_k \tag{5}$$

And the electric displacement tensor can be rewritten as

$$D_i = e_{ijk}u_{j,k} - \kappa_{ij}\phi_k \tag{6}$$

The force equilibrium should be satisfied in an elastic medium through the elastodynamic wave equation

$$C_{ijkl}u_{k,ll} + e_{kij}\phi_{kj} = \rho\ddot{u}_i \tag{7}$$

In the absence of volume charge, Maxwell's equation

$$\nabla \cdot D = 0 \tag{8}$$

must be satisfied. Combining this with expression of electric displacement field, the relation can be found as

$$e_{ijk}u_{j,ki} - \kappa_{ij}\phi_{ki} = 0 \tag{9}$$

Based on the differential equations derived above, both the host structure and transducers are modeled explicitly. The coupled formulation solves the mechanical equations of motion as an initial value problem and Maxwell's equation as a boundary value problem at each time step. The volume is spatially discretized in the three principal directions into a cuboidal grid, and the material properties of each cell are defined at the lower left front corner of the cell. While the material properties are constant within each cell, they are allowed to vary across cells, which enables the modeling of multilayer anisotropic and heterogeneous structures. The continuity of displacement is enforced at the nodes and traction across the interface by SIM (Paćko et al., 2012). To ensure convergence of the LISA/SIM technique, the time and three-dimensional space discretization satisfy the Courant–Friedrich–Lewy (CFL) condition. Meanwhile, the criterion that ensures at least eight elements per minimum wavelength is enforced to avoid amplitude distortions (Balasubramanyam et al., 1996).

All PZT sensors and actuators in this work are modeled as APC 850. In order to generate S0 and A0 modes individually, collocated actuation is implemented wherein two actuators are placed at the same location and on opposite sides of the plate (Su and Ye, 2004); the S0 mode with enhanced amplitude is generated by applying the voltages in opposite directions to actuators with respect to the centerline and the A0 mode with enhanced amplitude is generated by applying the voltages in the same direction with respect to the centerline. A zero-stiffness approximation is implemented to simulate the damaged region in any given layer.

A statistical TF analysis method, MPD (Mallat and Zhang, 1993), is used for post-processing and interpretation of the sensor signals. The TF features have been shown to provide highly localized characteristics of the time-varying spectral nature of damage wave-physics (Chakraborty et al., 2008). Due to the dispersive nature of guided wave, multiple modes are present in the TF domain in the high-frequency region (>300 kHz; for example, Figure 2); this complicates the task of identifying the desired mode in the signal. Therefore, a supervised learning based method is introduced to identify the A0 and S0 modes in the sensor signals based on the velocity estimation of each mode. This method is based on the dispersion property of the guided wave, known *a priori*, that the velocity of each mode is constant with a fixed product of the structure thickness and excitation frequency. First, a signal is collected from each sensor and transformed to the TF domain using the MPD algorithm. The ToF of each mode is found, and the group velocity is computed using the known distance between the sensors. The mode that maintains the same velocity is the desirable mode due to the nature of the guided wave. This mode selection technique is demonstrated by modeling a 16-layer UD CFRP with the dimension of 1200 mm × 300 mm × 1.6 mm. A set of 10 evenly distributed sensors are attached on the plate surface with a 100 mm distance between them, and the excitation frequency is set to be 500 kHz, as shown in Figure 1. Collocated actuation is used to

Figure 1. Contour for S0 mode with locations of sensors and actuator. Blue dot represents actuator and red dots represent sensors.

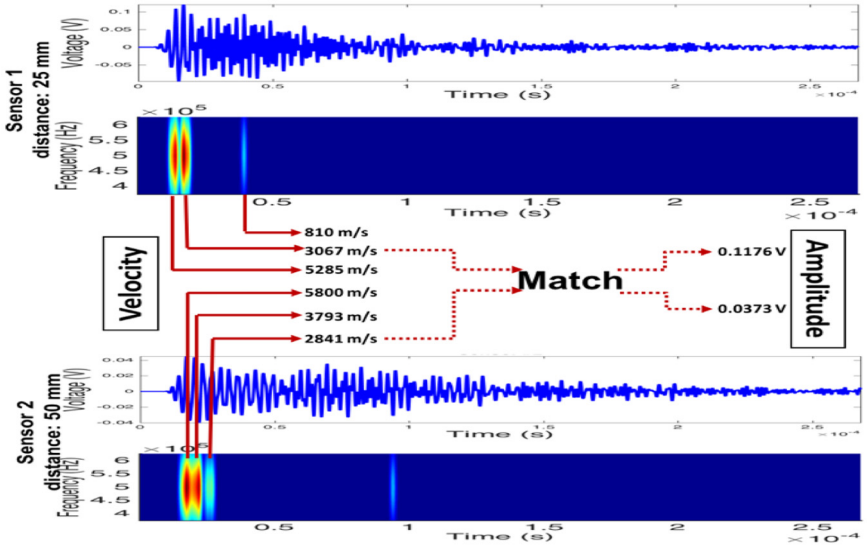

Figure 2. Output signal and its time–frequency representation for sensors 1 and 2.

selectively generate the S0 mode. The signals collected by the first two sensors and the corresponding time–frequency representations (TFRs) are shown in Figure 2. The exact location of the S0 mode cannot be identified because of the superposition of the first two existing modes. Thus, the group velocities of the decomposed wave packets are calculated with respect to the maximum amplitude location of the excitation signal. From the velocities of different modes shown in Figure 2, it is observed that the second mode in sensor 1 and the third mode in sensor 2 have velocities of around 3000 m/s, which indicates that this mode is the S0 mode. The velocity discrepancy at different sensors is due to the effect of the wave interaction with multiple sensors, which are explicitly modeled in the current framework. The initial modes in the signal can be attributed to the propagation of surface waves because the zero-order shear horizontal (SH0) wave (Su and Ye, 2004), which cannot propagate through the structural thickness, is also generated under the collocated actuation method. This method is then applied to model various composite laminates and sensor architectures containing multiple propagation and reflection modes. The method has shown good accuracy in mode identification. The detailed results and experimental comparisons are discussed in the sections that follow.

Guided wave propagation in composite panels

In this section, the behaviors of guided wave propagation in composite panels are investigated. The wave attenuation is studied by comparing the mode amplitudes extracted from varying propagation distances and orientations with respect to the actuator. The effects of varying excitation frequencies and material properties on the wave propagation are also discussed. At last, the model will be then used to evaluate the dispersion curves of CFRP and GFRP. Since the attenuation and dispersion characteristics play a significant role in optimizing sensor placement, the model can be used as an effective tool to minimize experimental efforts for wave based SHM framework.

Guided wave attenuation

To study the attenuation of S0 and A0 guided wave modes with distance, a CFRP UD plate with 16 layers

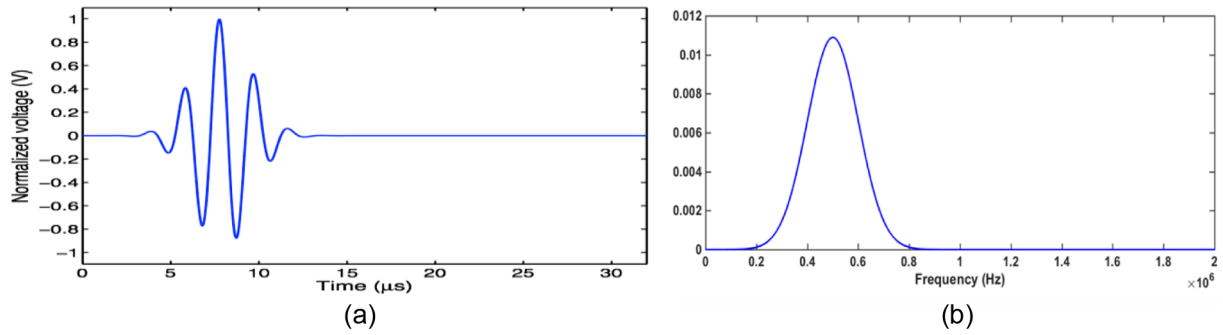

Figure 3. A 500-kHz five-cycle cosine tone burst excitation signal: (a) excitation signal and (b) frequency spectrum of excitation signal.

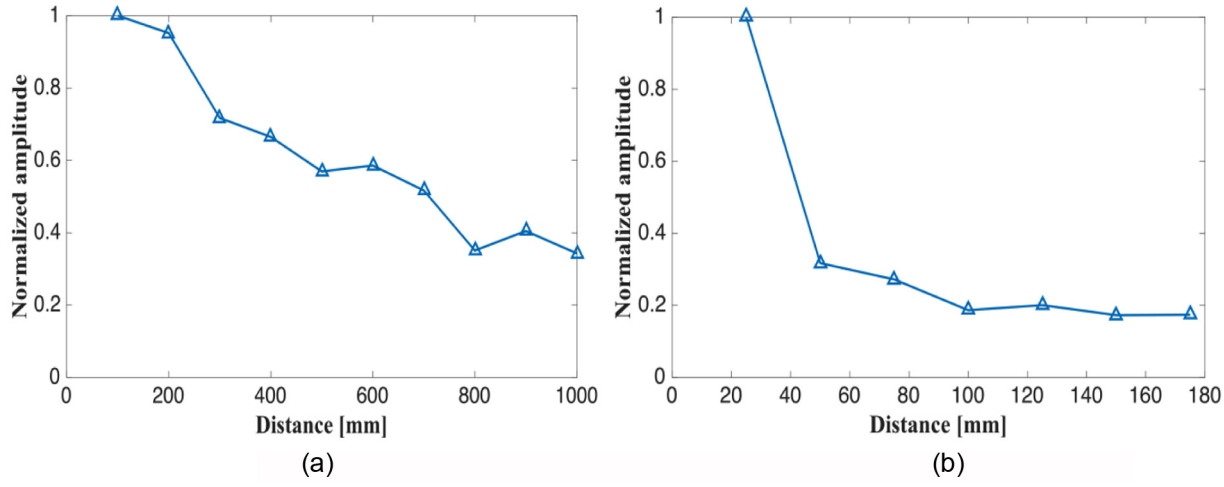

Figure 4. Amplitude attenuation of guided wave in UD CFRP with propagation distance: (a) S0 mode and (b) A0 mode.

$([0]_{8s})$ is modeled. The dimensions of the plate are 1200 mm × 300 mm × 1.6 mm. The actuator is located at 100 and 150 mm with respect to the bottom-left corner of the plate, and a total of 10 collinear sensors are placed at distances of 100–1000 mm from the actuator with an increment of 100 mm. A 500 kHz five-cycle cosine tone burst, shown in Figure 3, is used as the actuation signal. The frequency of 500 kHz has been used to compare the simulation results with the experimental work by Ono and Gallego (2012). A time step of 6.7×10^{-9} s and 0.1 mm three-dimensional spatial discretization are selected to ensure convergence of the LISA/SIM technique using the CFL condition, and a total of 4001 time steps have been used for 26.8 μs simulation time. The actuators are placed 100 mm away from the left edge to reduce boundary effect. The amplitudes of S0 and A0 mode are extracted from each sensor signal based on the supervised learning approach. Figure 4(a) and (b) shows the results, namely, the normalized A0 and S0 guided wave amplitudes as a function of propagation distance. The experimental results show that the normalized amplitude of S0 mode reduces to a value of 0.2 at sensing distance of 1000 mm, while the A0 mode reduces to the same value at sensing distance of 200 mm, indicating faster attenuation of the A0 mode. The simulation results presented in Figure 4 show similar trends as the experimental results of Ono and Gallego (2012).

Next, the attenuation with propagation distance in the QI CFRP composite plate with the same dimension as the UD plate is studied under the same excitation frequency, and the results are shown in Figure 5. Compared to Figure 4(a), it is observed that the S0 mode attenuates faster in QI CFRP than in the UD plate. This is due to the presence of fewer fibers along the propagation direction for the same fiber volume fraction as in the UD plate. However, the attenuation trend of the A0 mode remains the same, which indicates that the A0 mode is not sensitive to changes in the stacking sequence of the composite material. The stacking sequence governs the effective modulus of the composite panel (Maio et al., 2015) indicating that the material property changes have less impact on the velocity of A0 mode.

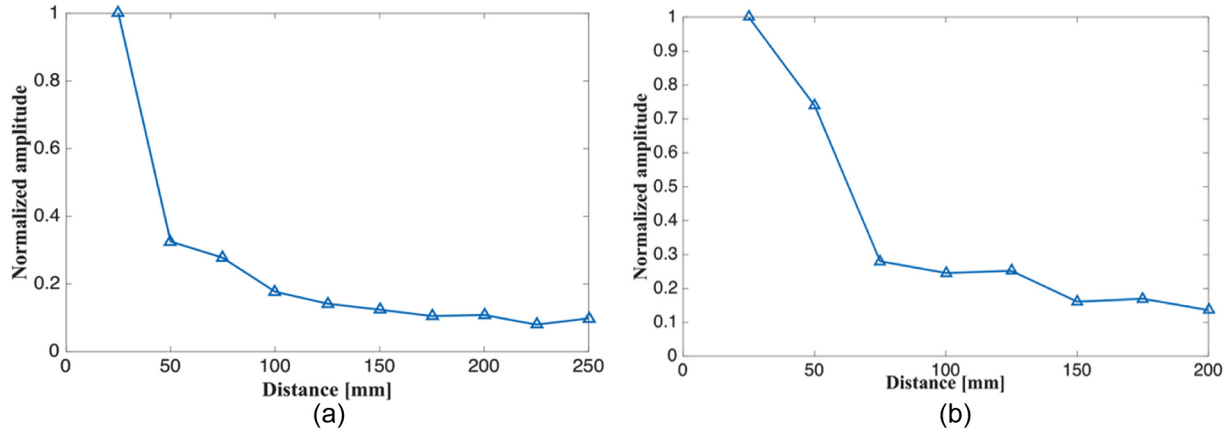

Figure 5. Amplitude attenuation of guided wave in QI CFRP with propagation distance: (a) S0 mode and (b) A0 mode.

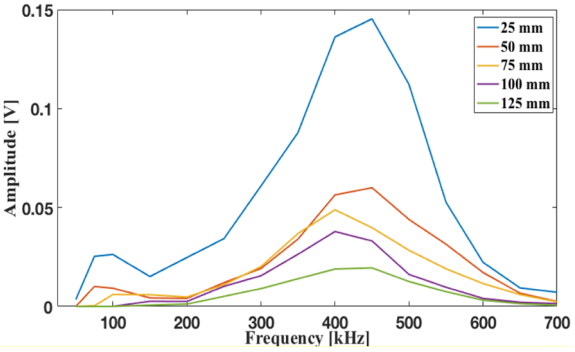

Figure 6. Attenuation at different frequencies for UD composite with varying distance between actuator and sensor.

Due to the dispersive nature of guided waves, the wave amplitude is also strongly dependent on the frequency. Therefore, it is necessary to study the effect of frequency on the attenuation trend. The same 16-layer UD layup is used to study the attenuation trend of S0 mode with varying frequency. The frequencies are varied between 50 and 700 kHz. Figure 6 shows that the S0 mode has the highest energy at a frequency range between 400 and 500 kHz, and the amplitude decreases to a very small value under low (<200 kHz) and high excitation (>600 kHz) frequency regions. In addition, the amplitude decreases with increasing sensor distance. These results are consistent with the experimental results of (Gresil and Giurgiutiu, 2013). The peaks observed in the simulation at small distances (25 and 50) mm in 100 kHz frequency region are due to the superposition of multiple modes that are closely spaced.

The effect of variation in material properties on the wave propagation behavior is studied next. A QI ($[0/45/–45/90]_{2s}$) laminate with three different types of fibers (AS-4, E-glass, Kevlar 49) and three different types of epoxy (Epoxy 3501-6, Epoxy HY6010, polyimides) are selected to generate five different fiber–epoxy material systems. The dimensions of all the models for the material properties study are 400 mm × 400 mm × 1.6 mm. The stiffness matrices of the five material systems and the material properties are extracted from the study of Daniel et al. (1994). The actuator is located at (100, 100) mm with respect to the bottom-left corner of the plate, and a total of four collinear sensors are placed at distances of 50, 100, 150, and 200 mm from the actuator. The excitation frequencies of all models for material sensitivity study are set to be 500 kHz.

First, the material properties of the matrix are changed while fibers (AS-4) remain the same; the actual and normalized attenuation trends are shown in Figure 7(a) and (b). The amplitude decreases with increasing sensor distance for all the three cases, and the attenuation trend is different for each material system, which illustrates the strong sensitivity of attenuation to matrix materials. Figure 7(c) and (d) shows the attenuation curves for material systems with varying fiber properties, while the matrix (Epoxy 3501-6) remains the same. The amplitude of the composite with E-glass fiber is significantly higher when compared to that of the other two types of fibers. This is because the E-glass fiber composite has the lowest modulus. Larger attenuation is also observed for the E-glass fiber and Kelvar49 systems compared to the AS-4 fibers due to their lower modulus. Comparing Figure 7(a) with Figure 7(c), the amplitudes for the three material systems in Figure 7(a) are almost the same because the fibers that dictate the wave propagation behavior are the same in these cases, while in Figure 7(c), the amplitudes change significantly due to change in fiber properties. Figure 8 provides the contours of out-of-plane displacement of the wave propagation in the five material systems at 45 μs. The wave propagations are almost symmetrical with respect to the actuator due to the QI composite layer-ups. The E-glass fiber has the lowest Young's modulus along the 0° wave propagation direction, which results in slower wave velocity in the 0° propagation direction as shown

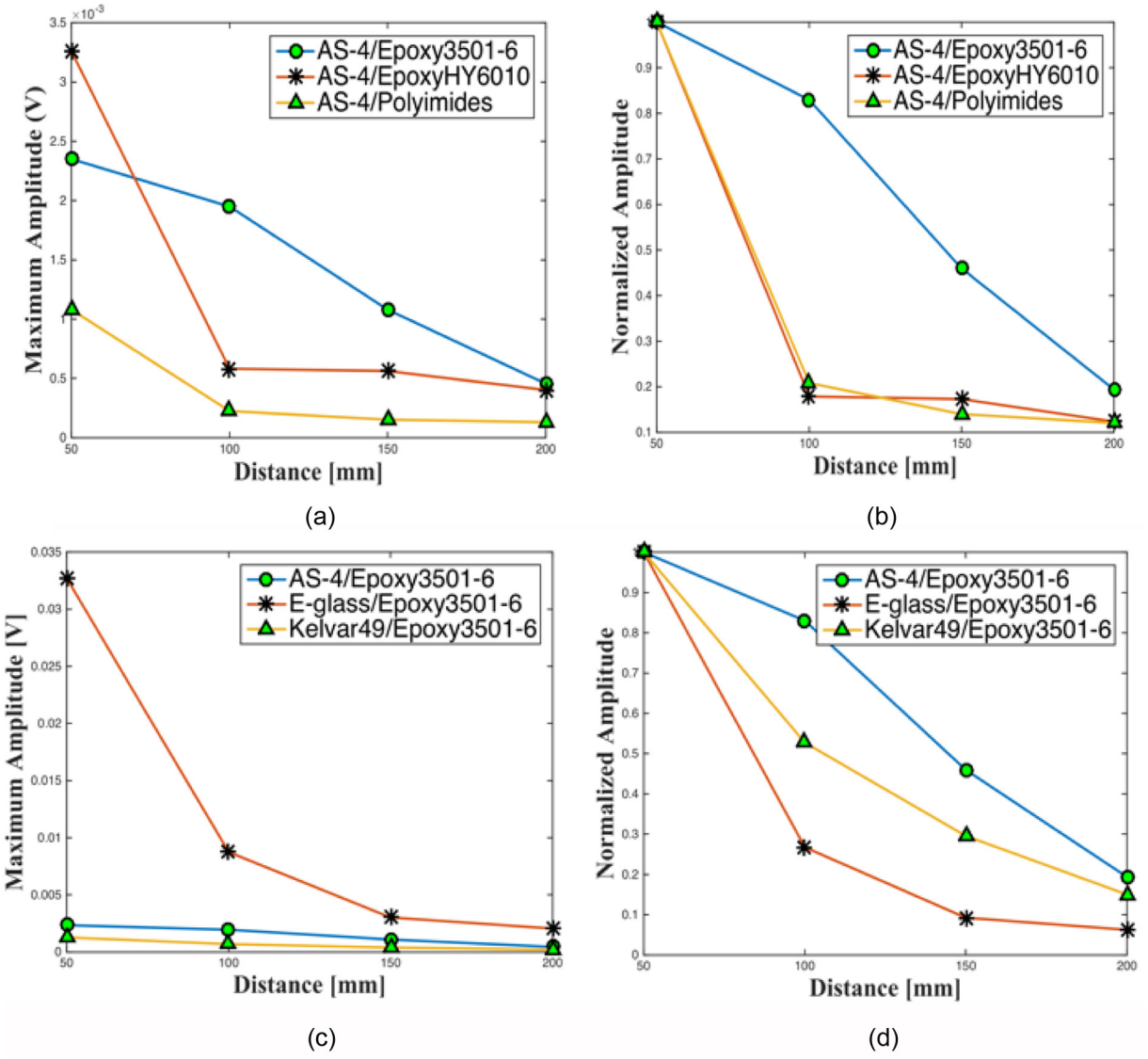

Figure 7. Effect of varying material properties: (a) varying epoxy properties, (b) normalized amplitude with varying epoxy properties, (c) varying fiber properties, and (d) normalized amplitude with varying fiber properties.

in Figure 8(d). These results indicate that the model outputs are consistent with theoretical elastic wave behavior.

A UD CFRP plate with nine collinear sensors placed at 100–900 mm from the actuator is modeled to study the effect of varying PZT material properties under the same excitation frequency and host structure. Three different cases are investigated, the original APC850 PZTs and PZTs with ±20% changes in properties. Figure 9 shows the normalized amplitude as a function of distance for the three cases. The wave amplitude decreases with increasing sensor distance, which is consistent with the results presented in the previous section. When the piezoelectric and dielectric properties are increased, the induced strain in the material increases due to increased transverse piezoelectric coefficient d_{31} leading to higher wave amplitude. Similarly, the amplitude reduces with decrease in piezoelectric and dielectric properties. This behavior is consistent with the theoretical electromechanical coupling relations.

The attenuation with respect to different propagation orientations is studied in plates with three different stacking sequences, UD, XP, and QI plates. The actuators are placed at the center of a 1000 mm × 1000 mm × 1.6 mm plate, and the sensors are placed at distances 50, 100, and 150 mm from the actuator. The excitation frequencies for directivity study are all set to be 500 kHz. The propagation direction is defined as the angle between the actuator and sensor with respect to the 0° fiber orientation. The amplitudes of S0 modes from sensors with different propagation angles are extracted and compared. Figure 10(a) shows the out-of-plane displacement contour of S0 mode propagation at 100 μs, and Figure 10(b) shows the attenuation

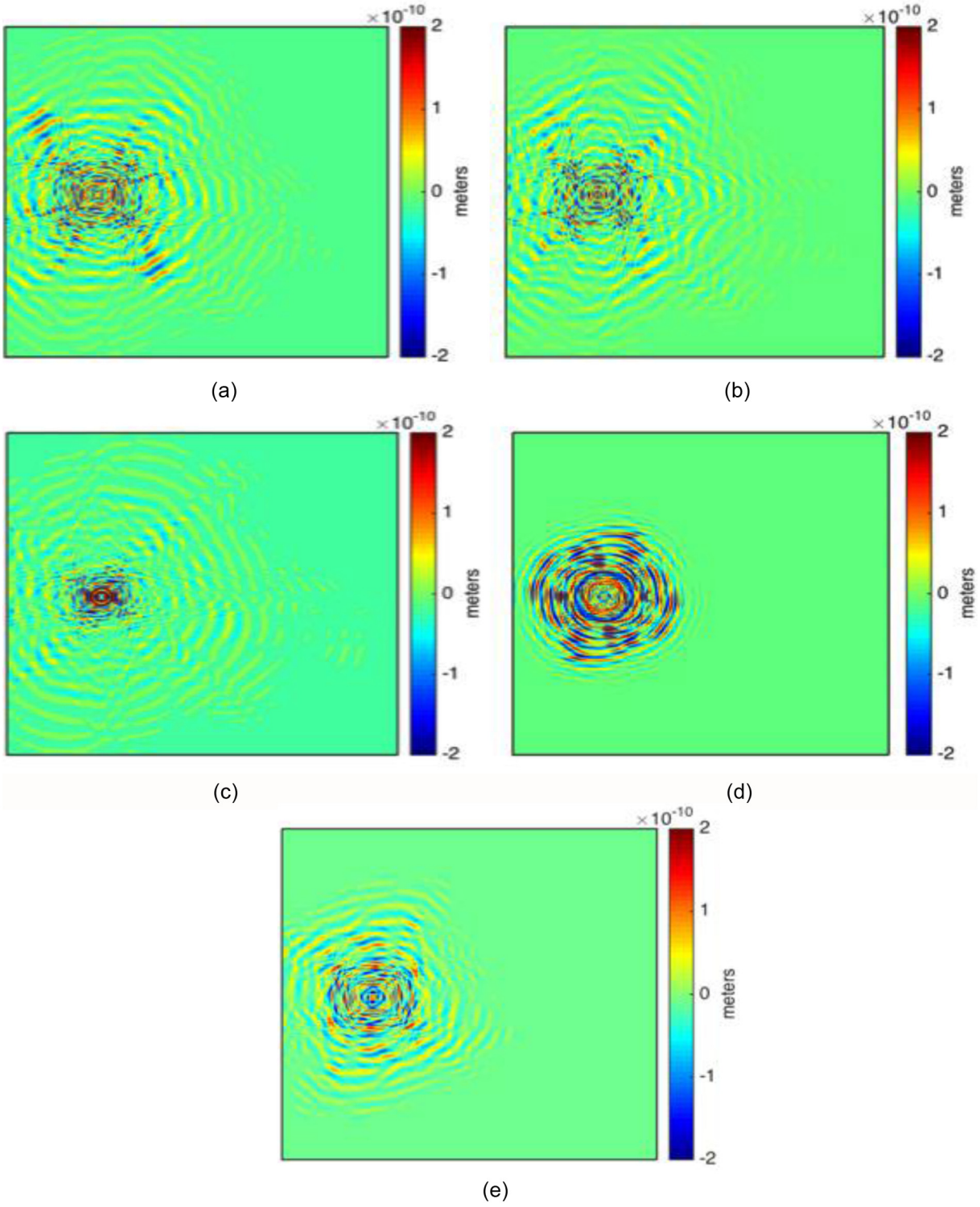

Figure 8. Wave propagation contours for different material systems at 45 μs: (a) AS-4/Epoxy3501-6, (b) AS-4/EpoxyHY6010, (c) AS-4/Polyimides, (d) E-glass/Epoxy3501-6, and (e) Kelvar49/Epoxy3501-6.

trend of S0 mode as a function of wave propagation direction in UD plate. The wave amplitude is maximum along the fiber direction and attenuates with increasing angle. This attenuation trend is consistent with the results (Ono and Gallego, 2012). The discrepancies in 50 mm simulation can be attributed to the mode superposition within a short propagation distance. For the XP plate, the amplitudes are studied from 0° to 180° with respect to the sensor. Figure 11(a) shows the out-of-plane displacement contour of S0

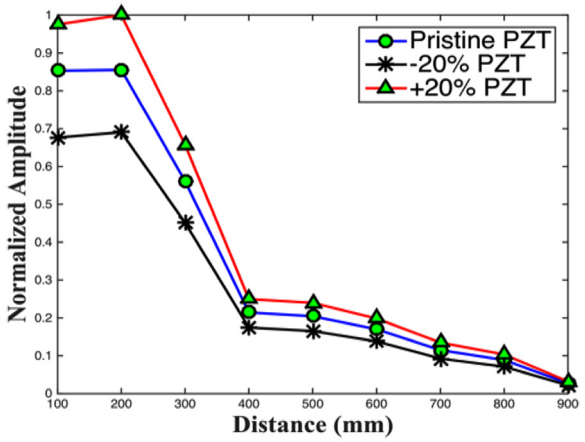

Figure 9. Attenuation curve with varying PZT properties.

mode propagation at 100.5 μs; the propagation distance is set to be 50 mm. The wave propagates faster along 0°, 90°, 180°, and 270° since the fibers are oriented along these directions. Figure 11(b) shows the attenuation trend as a function of the propagation angle. The peaks in amplitude are observed at 0°, 90°, and 180°, and the magnitudes in different propagation directions are highly symmetrical with respect to the fiber orientations. Two additional peaks are observed at 45° and 135° because the wave passes through equal number of 0° and 90° fibers along this direction so that the wave propagating along the 0° and 90° fibers interacts in these directions, which are the axis of symmetry to the fibers orientations. For S0 mode in QI CFRP, the sensor distance is varied between 50, 100, and 150 mm. The wave propagates faster along the fiber directions and since there are four different fiber

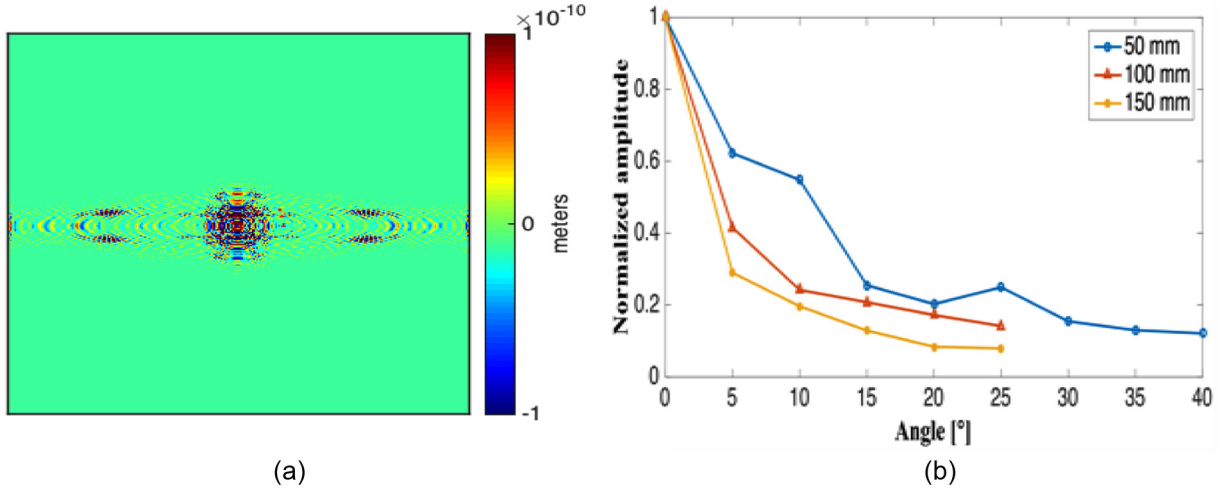

Figure 10. Directional attenuation in UD composites: (a) out-of-plane displacement contour and (b) directional attenuation.

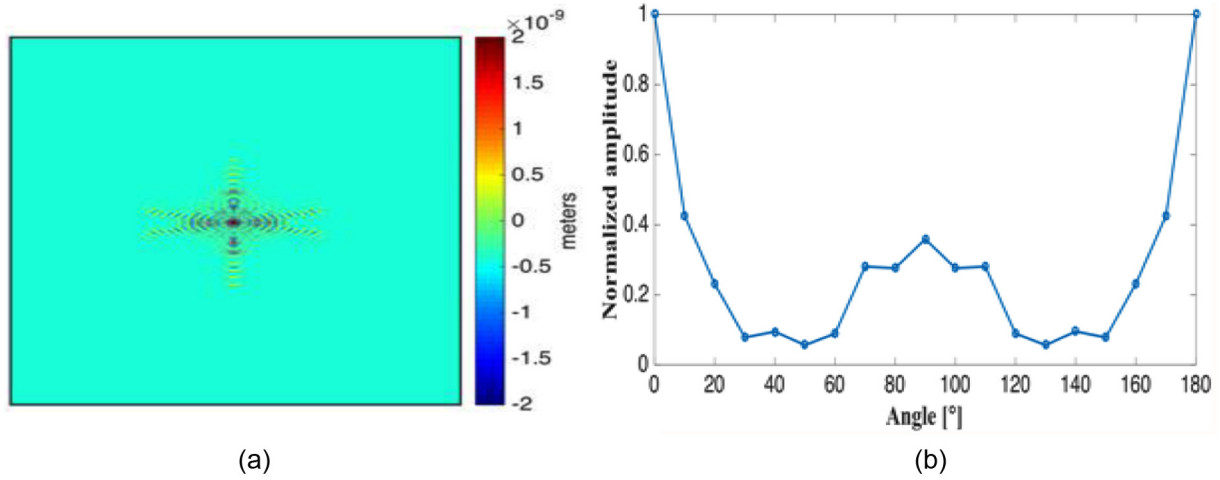

Figure 11. Directional attenuation in XP composites: (a) out-of-plane displacement contour and (b) directional attenuation.

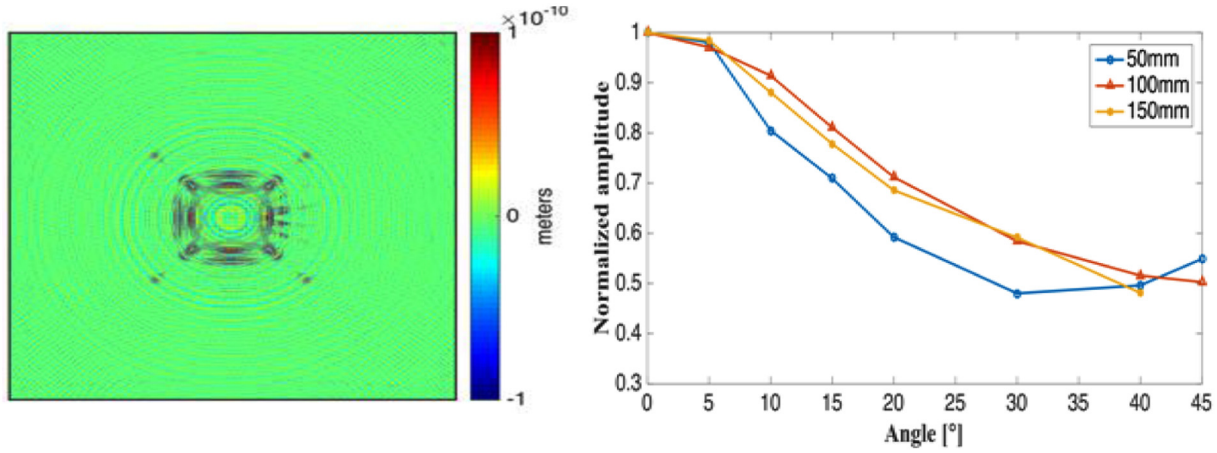

Figure 12. Directional attenuation in QI composites: (a) out-of-plane displacement contour and (b) directional attenuation.

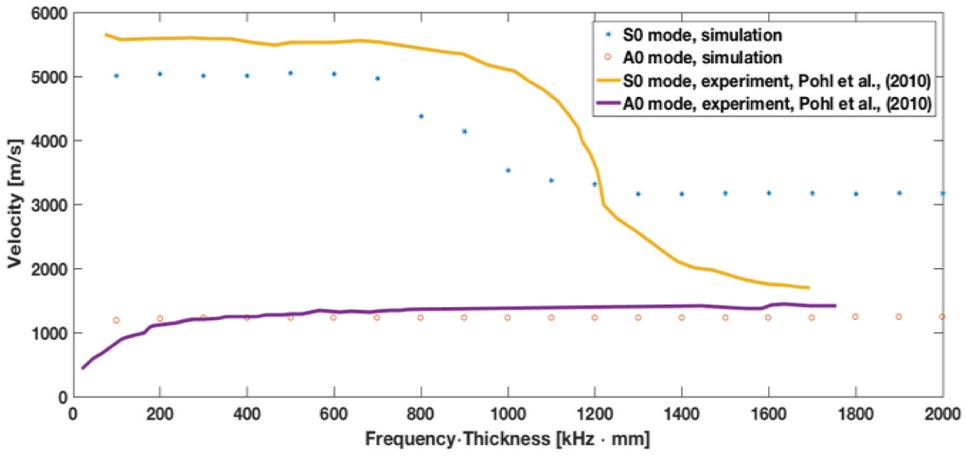

Figure 13. Dispersion curve of QI IM6/SCI081 CFRP.

orientations at any given point in the plate, the nature of the wave propagation is similar to that in an isotropic plate as shown in Figure 12(a). Figure 12(b) shows that the amplitude decreases when the propagation direction is away from the fiber orientation (0°) and then increases when it approaches another fiber orientation (45°) with a short propagation distance of 50 mm. However, when the distance increases to 100 mm, the amplitude decreases even with increasing propagation angle. This is because the longer propagation distance causes greater dispersive effect, which cannot be compensated by the presence of another fiber orientation.

Guided wave dispersion

In addition to damage, the material anisotropy, heterogeneity, and damping affect wave dispersion in composites. Therefore, the accuracy of estimating the dispersion curves using physics based models plays an important role in guided wave based SHM. The dispersion curves obtained from the numerical model are compared with the experimental results (Pohl et al., 2010). Two different composites, CFRP and GFRP, are modeled as QI seven-layer composite plates, $[(0/90)_f/45/-45/(0/90)_f]_s$, where "f" indicates the word "fabric." The dimension of the composite plates is 1300 mm × 300 mm × 2 mm, and the phase velocity of guided wave in a pre-determined 0° fiber orientation is computed. As shown in Figures 13 and 14, the trends of both A0 and S0 modes are similar to the experimental results. Figure 13 shows the dispersion curve of CFRP; the A0 velocity remains constant with respect to frequency change. The S0 mode remains constant when the value of the product of frequency and thickness is low (<600 kHz mm). A similar trend is observed at high values of frequency and thickness product (>1500 kHz mm). Since the three-dimensional

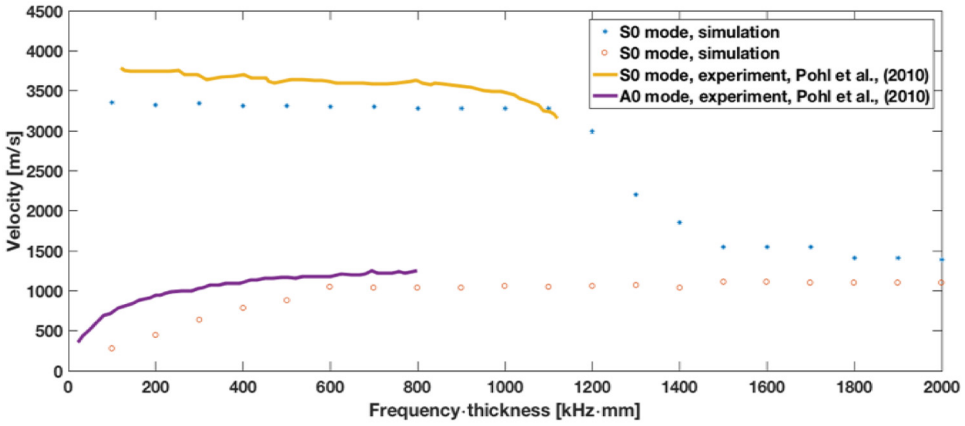

Figure 14. Dispersion curve of QI GFRP.

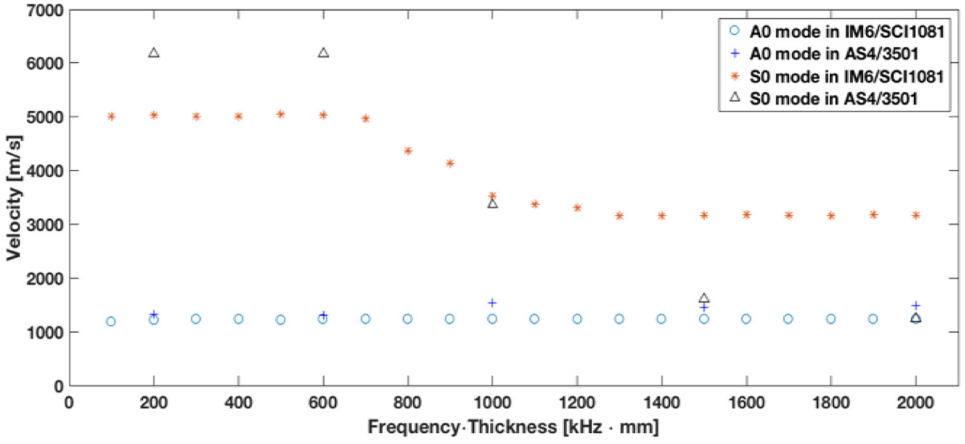

Figure 15. Comparison for dispersion curves with different carbon fiber composites.

material properties of the CFRP and GFRP used in the published work (Pohl et al., 2010) are not provided by the authors, a QI CFRP plate with IM6/SCI081 carbon fibers is used in the simulation. However, good agreement is observed between the simulation and experiments in the cases of both CFRP and GFRP plates. The discrepancy observed from the dispersion curve of CFRP is due to the mismatch of material properties.

To quantify the effect of varying material property on the guided wave velocity, two different types of QI carbon fibers composites, IM6/SCI081 and AS-4/3501-6, are modeled. Five different frequencies corresponding to the frequency thickness products of 200, 600, 1000, 1500, and 2000 kHz mm are investigated as shown in Figure 15. The results indicate that the S0 mode is highly sensitive to the varying materials and shows significant variation in velocity for the two different layups. The A0 mode velocity almost remains the same over the frequency thickness range of 200–2000 kHz mm. Next, a UD AS-4/3501-6 composite panel is modeled, and the effect of individual stiffness components (E1, E2 and G12) on the wave velocity are studied by sequentially introducing a 3% perturbation in each of the component; and the results are summarized in Table 1. The results indicate that the small perturbations in the stiffness values cause significant changes in velocities of both S0 and A0 mode; note that the velocity change of S0 modes, between the cases with and without perturbations, is larger than that of A0 mode.

Damage assessment in composite panels

The primary purpose of developing the simulation framework is to study the changes in wave propagation and the signals in the presence of damage. A 16-layer ($[0]_{8s}$) CFRP UD plate with dimensions of 1200 mm $\times$ 300 mm $\times$ 1.6 mm is modeled, and a 500-kHz five-cycle cosine tone burst is used for excitation based on the amplitude–frequency relation discussed in section "Guided wave attenuation". Collocated methodology, introduced in section "Modeling approach", is used to assess the signal changes of symmetric and

Table 1. Velocities from perturbations in material properties.

Wave mode	E1		E2		G12	
	S0 (m/s)	A0 (m/s)	S0 (m/s)	A0 (m/s)	S0 (m/s)	A0 (m/s)
3% decrease	8830	898	8740	889	8740	882
Pristine	8900	905	8900	905	8900	905
3% increase	8990	911	8990	914	8990	921

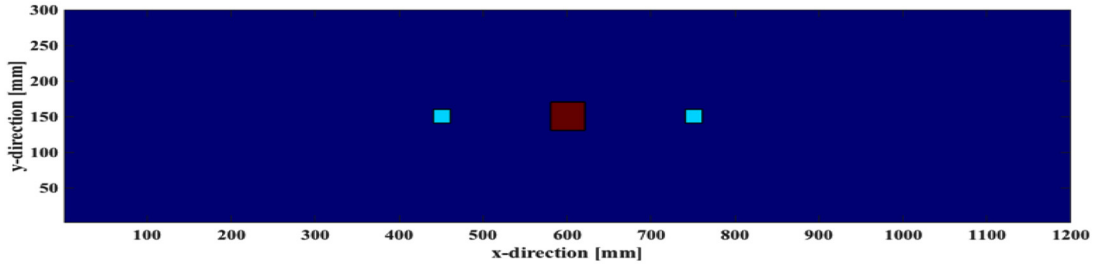

Figure 16. Representation of locations of transducers and damage (light blue: actuator and sensor, red: damage).

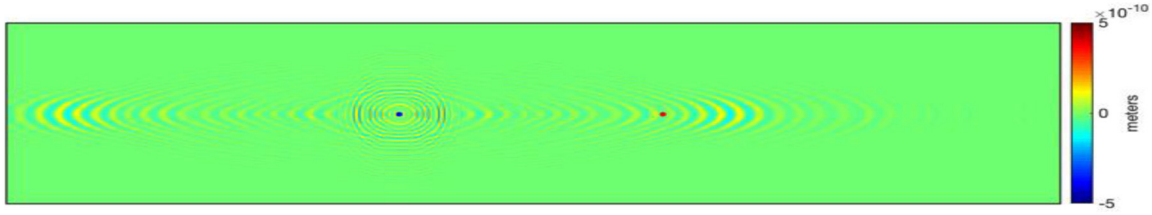

Figure 17. Contour for symmetric wave propagation; blue dot represents actuator, and red dots represent sensors.

anti-symmetric modes in the presence of damages. As shown in Figure 16, the actuator is placed at the location (450, 150) mm and the sensor is placed at (750, 150) mm at the surface of the composite panel. The damages (40 mm × 40 mm) are positioned in the middle of the sensor and actuator and at the following ply interfaces: 1st layer, the mid-layer (9th layer), and the 16th, respectively.

Symmetrically collocated methodology

To assess the signal changes under symmetrically collocated excitation due to damage, the wave propagation without damage is investigated first. The wave propagation at 112.5 μs is shown in Figure 17, and the output signal and corresponding TF representation is shown in Figure 18(a). It can be observed that there are three major wave envelopes with the highest amplitude, which also contain relatively larger energy than other envelopes. These envelopes, circled in red in Figure 18(a), are chosen, and the ToF and amplitudes are extracted by MPD methodology to serve as the baseline in the damage assessment study.

The sensor signals and the corresponding TFRs for all cases (healthy and three damaged cases) are presented in Figure 18 and show the quantitative changes in the damage cases. The amplitudes of all the existing wave modes are extracted, and the TFRs are presented for the five wave modes with the highest amplitudes. It should be noticed that due to the mode conversion and attenuation effects, the five modes that have the highest amplitudes are different in each damaged cases. Compared with the healthy case, the three selected envelope shapes of signals do not change significantly if the damage is in the first layer. But the dispersion effects in the three envelopes can be clearly observed. However, when the damage is at mid-layer, the signal changes significantly. Comparing the TFRs between Figure 18(a) and (c), the first two selected envelopes split into multiple lower energy envelopes. Furthermore, the three selected envelopes have a large dispersive effect, which results in a later arrival time of envelope peak compared to the other damage cases. The waveforms of output sensor signal from the plate with damage at the 16th layer are very similar to the signal output from the healthy plate. The signal features (ToF and amplitude) are compared with baseline data, which are summarized in Table 2. The data indicate there is a ToF delay due to the presence of damage

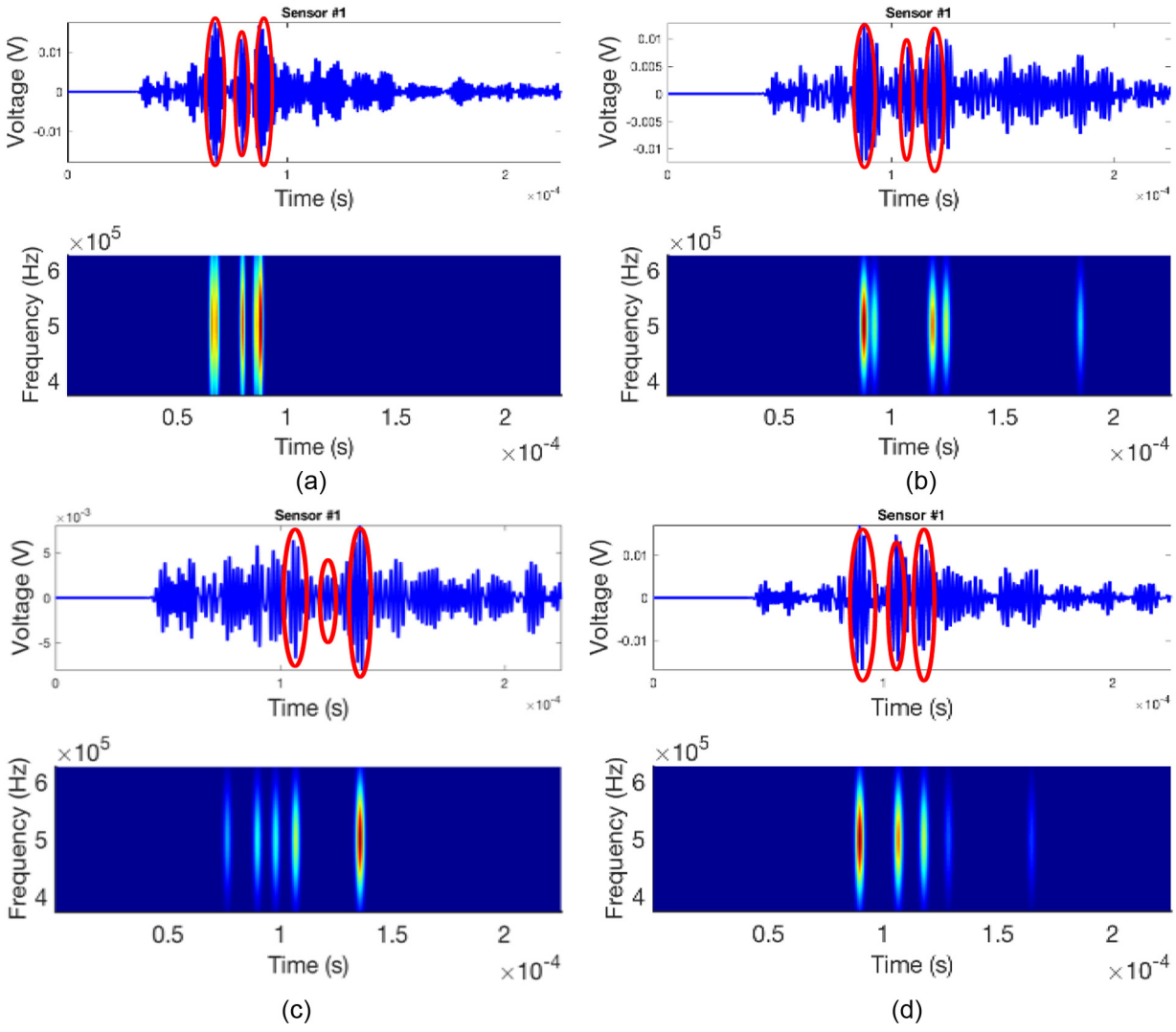

Figure 18. Signals and TFRs under symmetric excitation with damages at different through-thickness locations (red circles indicate the wave envelopes to be assessed): (a) healthy plate, (b) damage at 1st layer, (c) damage at 9th layer, and (d) damage at 16th layer.

Table 2. Amplitude and signal comparison from different locations of damages for symmetric excitation.

Damage location	First envelope		Second envelope		Third envelope	
	AMP (V)	ToF (μs)	AMP (V)	ToF (μs)	AMP (V)	ToF (μs)
Health	0.018	68	0.016	80	0.017	88
Layer #1	0.013	90	0.009	107	0.011	118
Layer #9	0.006	89	0.007	107	0.008	140
Layer #16	0.017	91	0.015	107	0.012	118

AMP: amplitude; ToF: time of flight.

between actuator and sensor; the ToF appears to be insensitive to the through-thickness location. However, it can be seen that the amplitudes of selected modes are highly sensitive to the location of damage in the through-thickness direction. When the damage is at the 1st layer, there is a larger amplitude reduction compared to that from the plate with damage in the 16th layer, particularly since there is more attenuation effect on the surface wave. Moreover, for the case with the damage at mid-layer, the amplitudes of all selected envelopes are reduced significantly due to the damage. It can be interpreted as follows: the mode separation and dispersion effects reduce the energy contained in the selected envelopes, resulting in reduced amplitudes

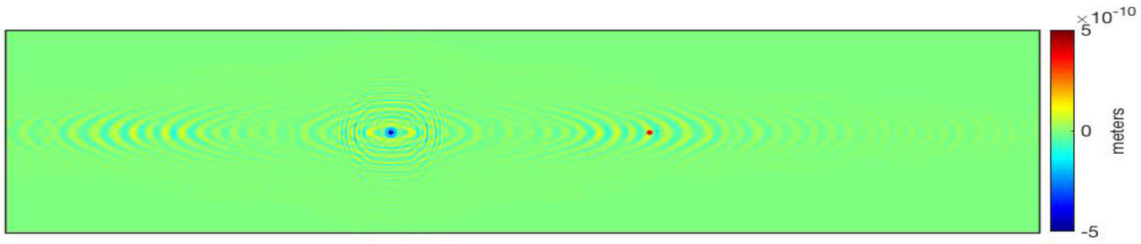

Figure 19. Contour for anti-symmetric wave propagation; blue dot represents actuator, and red dots represent sensors.

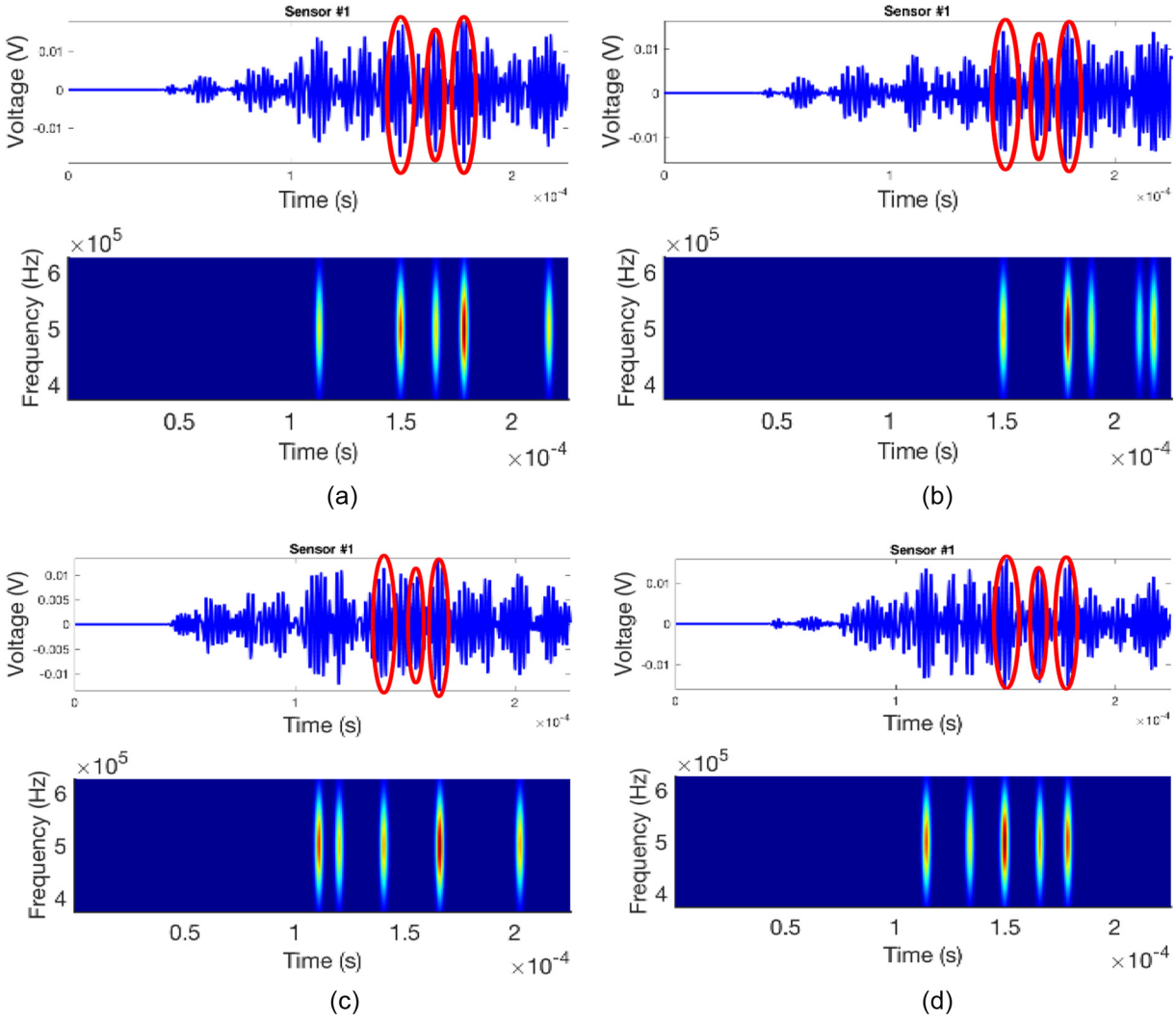

Figure 20. Signals and TFRs under anti-symmetric excitation with damages at different through-thickness locations (red circles indicate the wave envelopes to be assessed): (a) healthy plate, (b) damage at 1st layer, (c) damage at 9th layer, and (d) damage at 16th layer.

in case of the deeply seeded damage, when compared to the damage at the 1st layer.

Anti-symmetrically collocated methodology

The ability of anti-symmetrically collocated excitation for damage assessment is examined, and the signal changes (for the same plate and damage cases) are compared with those from the symmetrically collocated methodology. The wave propagation of the baseline (healthy) plate at 112.5 μs is shown in Figure 19, and the output signal and corresponding TF representation is presented in Figure 20(a). Similar to the symmetric collocation case, there are three major wave envelopes

Table 3. Amplitude and ToF comparison from different locations of damages for anti-symmetric excitation.

Damage location	First envelope		Second envelope		Third envelope	
	AMP (V)	ToF (μs)	AMP (V)	ToF (μs)	AMP (V)	ToF (μs)
Health	0.017	150	0.016	166	0.019	178
Layer #1	0.014	150	0.011	166	0.015	178
Layer #9	0.010	149	0.013	166	0.008	177
Layer #16	0.016	150	0.015	166	0.015	178

AMP: amplitude; ToF: time of flight.

with the highest amplitude and energy (shown with red circles in Figure 20(a)); the corresponding ToF and amplitudes, extracted using MPD, are used in the damage assessment study.

In order to investigate further differences between the ability of these two excitation techniques and to establish the reliability of the SHM framework, the sensor signals from the healthy and the damaged plates (Figure 20(a) to (d)) are compared. As mentioned in section "Symmetrically collocated methodology", the TFRs are presented for the five wave modes with the highest amplitudes, and MPD methodology is used to extract the amplitudes of all existing wave modes. For the plate with damage in the first layer (Figure 20(b)), the amplitudes of all three selected envelopes are reduced. However, compared to the symmetric case, the dispersion effects are minor, and all the three envelopes maintain similar shapes. Comparing the TFRs between Figure 20(a) and (c), the signal from the plate with damage at mid-layer demonstrates a more complex behavior; the first envelope shows significant dispersion, the second envelope maintains the same shape with a small amplitude reduction, and the third envelope experiences significant amplitude reduction. The sensor signal from the plate with damage at the 16^{th} layer closely resembles the signal from the healthy plate. The signal features (ToF and amplitude) are summarized in Table 3. The data indicate that there is no ToF delay due to damage in the selected modes, which means that in this particular case, the ToF does not provide useful information for damage identification and localization. The amplitudes of selected modes, however, show high sensitivity and can be used to identify the location of through-thickness damages. A larger amplitude reduction is observed when the delamination is at the 1^{st} layer, compared to the case where it is located at the 16^{th} layer, except for the 3rd envelope. For the case with the damage at mid-layer, the amplitude and ToF indicates that (1) the amplitudes of the first envelope reduces significantly due to the dispersion effect as mentioned before, (2) the amplitude reduction of the second envelope is lower compared to the plate with 1^{st} layer damage but larger than that from the plate with 16^{th} layer damage, (3) the amplitude of the third envelope is reduced a lot more when damage is at the mid-layer compared with other cases, which indicates this envelope is also highly sensitive to mid-layer damage.

Summary

A computationally efficient and generalized three-dimensional numerical model is developed to simulate wave propagation in anisotropic composite structures. A TF analysis technique, MPD, is used in conjunction with a supervised learning based velocity estimation method to accurately calculate the ToF and velocities of existing wave modes. Wave attenuation and dispersion are studied under varying composite layups, excitation frequencies, excitation modes (symmetric and anti-symmetric), and material properties of composite panels and PZTs using a three-dimensional numerical simulation technique that accounts for electromechanical coupling between the host structure and the transducers. The sensitivity study of material property indicates that the fiber material properties have a larger effect on wave propagation compared to matrix properties. Comparing with symmetric mode, the anti-symmetric guided wave mode shows less sensitivity to the changes of material properties. The mechanism of interaction between ultrasonic wave and damage is also studied. With a fixed geometry and excitation frequency, the signal changes due to varying damage locations along the through-thickness direction are compared under both symmetrically and anti-symmetrically collocated excitations. The results show that the amplitude changes in both excitation methodologies have the potential to identify and quantify the structural damages, while the symmetrically collocated excitation method is more sensitive to ToF based damage detection method. In conclusion, the current model is capable of accurately modeling the behavior of guided waves in composite materials and can be used as an effective tool in sensor placement optimization, damage identification, and localization to reduce the experimental efforts in guided wave based SHM framework.

Acknowledgements

The authors thank Dr. Cenek Sandera, Technical Monitor, for the support of this work.

Declaration of conflicting interests

The author(s) declared no potential conflicts of interest with respect to the research, authorship, and/or publication of this article.

Funding

The author(s) disclosed receipt of the following financial support for the research, authorship, and/or publication of this article: This work was supported by the Honeywell International s.r.o. in the Czech Republic, under Grant RPS dated 07/28/169.

References

Ali R, Mahapatra DR and Gopalakrishnan S (2005) Constrained piezoelectric thin film for sensing of subsurface cracks. *Smart Materials and Structures* 14(2): 376–386.

Balasubramanyam R, Quinney D, Challis RE, et al. (1996) A finite-difference simulation of ultrasonic Lamb waves in metal sheets with experimental verification. *Journal of Physics D: Applied Physics* 29(1): 147–155.

Borkowski L, Liu K and Chattopadhyay A (2013) Fully coupled electromechanical elastodynamic model for guided wave propagation analysis. *Journal of Intelligent Material Systems and Structures* 24(13): 1647–1663.

Chakraborty D, Soni S, Wei J, et al. (2008) Physics based modeling for time-frequency damage classification. In: *International Symposium on Smart Structures and Materials & Nondestructive Evaluation and Health Monitoring* 6926: 69260M.

Chillara VK and Lissenden CJ (2014) Nonlinear guided waves in plates: a numerical perspective. *Ultrasonics* 54: 1553–1558.

Corigliano A (1993) Formulation, identification and use of interface models in the numerical analysis of composite delamination. *International Journal of Solids and Structures* 30(20): 2779–2811.

Daniel IM, Ishai O, Daniel IM, et al. (1994) *Engineering Mechanics of Composite Materials*. New York: Oxford University Press.

Delsanto PP (1998) A spring model for the simulation of the propagation of ultrasonic pulses through imperfect contact interfaces. *Journal of the Acoustical Society of America* 1045: 2584–2591.

Delsanto PP, Schechter RS and Mignogna RB (1997) Connection machine simulation of ultrasonic wave propagation in materials, III: the three-dimensional case. *Wave Motion* 26(4): 329–339.

Delsanto PP, Schechter RS, Chaskelis HH, et al. (1994) Connection machine simulation of ultrasonic wave propagation in materials, II: the two-dimensional case. *Wave Motion* 20(4): 295–314.

Delsanto PP, Whitcombe T, Chaskelis HH, et al. (1992) Connection machine simulation of ultrasonic wave propagation in materials, I: the one-dimensional case. *Wave Motion* 16(1): 65–80.

Farrar CR and Worden K (2007) An introduction to structural health monitoring. *Philosophical Transactions of the Royal Society of London, Series A: Mathematical, Physical and Engineering Sciences* 365: 303–315.

Giurgiutiu V (2007) *Structural Health Monitoring: With Piezoelectric Wafer Active Sensors*. San Diego, CA: Academic Press.

Gresil M and Giurgiutiu V (2013) Guided wave propagation in carbon composite laminate using piezoelectric wafer active sensors. In: *SPIE Smart Structures and Materials+ Nondestructive Evaluation and Health Monitoring* 8695: 869525.

Kijanka P, Radecki R, Packo P, et al. (2013) GPU-based local interaction simulation approach for simplified temperature effect modelling in Lamb wave propagation used for damage detection. *Smart Materials and Structures* 22(3): 035014.

Koshiba M, Karakida S and Suzuki M (1984) Finite-element analysis of Lamb wave scattering in an elastic plate waveguide. *IEEE Transactions on Sonics and Ultrasonics* 31(1): 18–24.

Leckey CA, Rogge MD and Raymond Parker F (2014) Guided waves in anisotropic and quasi-isotropic aerospace composites: three-dimensional simulation and experiment. *Ultrasonics* 54(1): 385–394.

Liu Y, Mohanty S and Chattopadhyay A (2010) Condition based structural health monitoring and prognosis of composite structures under uniaxial and biaxial loading. *Journal of Nondestructive Evaluation* 29(3): 181–188.

Liu Z, Oswald J and Belytschko T (2013) XFEM modeling of ultrasonic wave propagation in polymer matrix particulate/fibrous composites. *Wave Motion* 50(3): 389–401.

Lu Y, Ye L and Su Z (2006) Crack identification in aluminium plates using Lamb wave signals of a PZT sensor network. *Smart Materials and Structures* 15(3): 839–849.

Maio L, Memmolo V, Ricci F, et al. (2015) Ultrasonic wave propagation in composite laminates by numerical simulation. *Composite Structures* 121: 64–74.

Mallat SG and Zhang Z (1993) Matching pursuits with time-frequency dictionaries. *IEEE Transactions on Signal Processing* 41(12): 3397–3415.

Marklein R (1999) The finite integration technique as a general tool to compute acoustic, electromagnetic, elastodynamic, and coupled wave fields. *Review of Radio Science* 2002: 201–244.

Mohanty S, Chattopadhyay A and Peralta P (2010) Adaptive residual useful life estimation of a structural hotspot. *Journal of Intelligent Material Systems and Structures* 21(3): 321–335.

Nadella KS and Cesnik CE (2013) Local interaction simulation approach for modeling wave propagation in composite structures. *CEAS Aeronautical Journal* 4(1): 35–48.

Nayfeh AH (1991) The general problem of elastic wave propagation in multilayered anisotropic media. *Journal of the Acoustical Society of America* 89(4): 1521–1531.

Neerukatti RK, Hensberry K, Kovvali N, et al. (2016) A novel probabilistic approach for damage localization and prognosis including temperature compensation. *Journal of Intelligent Material Systems and Structures* 27(5): 592–607.

Neerukatti RK, Liu KC, Kovvali N, et al. (2014) Fatigue life prediction using hybrid prognosis for structural health monitoring. *Journal of Aerospace Information Systems* 11(4): 211–232.

Obenchain MB and Cesnik CE (2013) Producing accurate wave propagation time histories using the global matrix method. *Smart Materials and Structures* 22(12): 125024.

Ono K and Gallego A (2012) Attenuation of lamb waves in CFRP plates. *Journal of Acoustic Emission* 30: 109–123.

Paćko P, Bielak T, Spencer AB, et al. (2012) Lamb wave propagation modelling and simulation using parallel processing architecture and graphical cards. *Smart Materials and Structures* 21(7): 075001.

Pohl J, Mook G, Lammering R, et al. (2010) Laser-vibrometric measurement of oscillating piezoelectric actuators and of Lamb waves in CFRP plates for structural health monitoring. In: *AIP Conference Proceedings* 1253: 65–72.

Pruell C, Kim JY, Qu J, et al. (2009) A nonlinear-guided wave technique for evaluating plasticity-driven material damage in a metal plate. *NDT & E International* 42(3): 199–203.

Raghavan A and Cesnik CE (2007) Review of guided-wave structural health monitoring. *The Shock and Vibration Digest* 39(2): 91–116.

Rudd KE, Leonard KR, Bingham JP, et al. (2007) Simulation of guided waves in complex piping geometries using the elastodynamic finite integration technique. *Journal of the Acoustical Society of America* 121(3): 1449–1458.

Seaton CT, Mai X, Stegeman GI, et al. (1985) Nonlinear guided wave applications. *Optical Engineering* 24(4): 244593.

Staszewski WJ, Lee BC and Traynor R (2007) Fatigue crack detection in metallic structures with Lamb waves and 3D laser vibrometry. *Measurement Science and Technology* 18(3): 727–739.

Su Z and Ye L (2004) Selective generation of Lamb wave modes and their propagation characteristics in defective composite laminates. *Proceedings of the Institution of Mechanical Engineers, Part L: Journal of Materials Design and Applications* 218(2): 95–110.

Talbot JR and Przemieniecki JS (1975) Finite element analysis of frequency spectra for elastic waveguides. *International Journal of Solids and Structures* 11(1): 115–138.

Thostenson ET, Li WZ, Wang DZ, et al. (2002) Carbon nanotube/carbon fiber hybrid multiscale composites. *Journal of Applied Physics* 91(9): 6034–6037.

Todoroki A, Omagari K, Shimamura Y, et al. (2006) Matrix crack detection of CFRP using electrical resistance change with integrated surface probes. *Composites Science and Technology* 66(11): 1539–1545.

Zienkiewicz OC, Taylor RL and Fox DD (2013) *The Finite Element Method for Solid and Structural Mechanics*. Oxford: Butterworth-Heinemann.